Application of CUK and ZETA Dc-Dc Choppers for Power Factor Correction and Power Quality Improvement of BLDC Motor

Syed. Siddik, G. JogaRao, D.V.N. Ananth

***Abstract*: For industrial, electrical vehicles, drives, and grid applications ac-dc based inverters with power factor correction is considered as a key element to meet the power system firm regulatory rules. Among these dc-ac inverters, bridgeless converters play a vital role. In this paper, Bridgeless cuk and zeta converter-fed brushless dc (BLDC) motor drive is studied for power factor correction (PFC) and power quality improvement. The major objectives of this work are (i) dc bulk capacitance and inductance use is decreased, so that permanence film capacitors can be utilized, (ii) overall efficiency of BLDC drive system is improved due to decreased losses in the switches and conducting devices and (iii) guaranteed high or unity source power factor. The motor and source parameters are examined in this study for PFC using CUK and ZETA based dc-dc converters with MATLAB software. The work is compared with bridgeless ZETA, CUK and**

Keywords: bridgeless converter, ZETA dc-dc converter, CUK dc-dc converter, power factor correction.

I. INTRODUCTION

The industrial loads especially motor drives, electric furnace and many commercial loads like electrical vehicles, automatic lighting and control systems uses dc-ac inverter systems [1]. This inverter uses semiconductor switches like IGBTs which will induce large difference in the power factor when using these loads and hence there is a necessity for power factor correction [2] and [3]. As the government regulations, low power factor in source supply pose penalty on the firm and also is a bad remark [4]. This low power factor also leads to light flickering and poor performance of the other sensitive loads. So, buck-boost or some combinational chopper based inverter devices plays a vital role [5]. These are classified mainly as bridged boost and bridgeless converters [6] and [7]. The bridged boost power factor correction (PFC) devices are simple in construction, easy to implement, low cost, unity factor achievement and reliable [8]. However, conduction losses will be increased drastically in continuous conduction mode because of diode bridge rectifier and therefore losses of the overall system increases, more heat is generated. So, long-time operation will damage the switches. The bridgeless or dual-boost converters which do not have diode bridge drives will offer all the above said advantages and also low switching and conduction losses as this configuration do not have a diode bridge rectifier. These devices use only a single isolated- current sensor and are an added advantage. The use of these bulk capacitors are replaced using the logic, a dual cascaded dc to dc conversion operation, one for dc voltage level changing and the other for PFC [9-11]. Here, both the dc converters are separated by a common dc link capacitor operated at higher frequency. Beyond many advantages as said above, this configuration, the major drawbacks are considerable losses in each stage.

With the same dual cascaded chopper configuration, the overall efficiency can be achieved by using soft-switching logic which reduces the switching and conducting losses. Inrush currents, surge voltage, rapid mode change from continuous to discontinuous and vice-versa etc. The other approach is using interleaved bridgeless choppers like SEPIC [12], [13], CUK [14], [15], LUO [16], ZETA [17-19], etc. The interleave choppers consist of two parallel stage converters while among them one is a bigger structure one, is complex in design. However, practical prototype is very easy, uses more distribution passive components so heat dissipation is easy, reduced conduction losses and hence overall efficiency and reliability is increased and target of PFC can be achieved easily. The current flow path also is reduced with this type of configuration. Comparison of bridged and bridgeless converters is done to understand performance and efficiency characteristics of the converters, drives and overall system [20]. A Multi-Carrier Modulation Technique for BLDC motor is explained in [21]. The buck-boost, CUK, single ended primary inductance converter (SEPIC), LUO, ZETA type bridgeless power factor correction converter topologies are extensively discussed in the literature with their design, modelling and implementation. These devices offer better dynamic response, low switching losses, and improved source sinusoidal current waveform. The major objectives of this work are (i) dc bulk capacitance and inductance use is decreased, so that permanence film capacitors can be utilized, (ii) overall efficiency of BLDC drive system is improved due to decreased losses in the switches and conducting devices and (iii) guaranteed high or unity source power factor. The objective of the paper is to use ZETA converter fed BLDC motor drive in order to improve the power quality at the supply by reducing the total harmonic distortion factor and increasing power factor to unity. And also by adjusting the dc link voltage of the voltage source inverter (VSI) feeding a BLDC motor, the speed of the BLDC motor is controlled.

Revised Manuscript Received on July 22, 2020.

Syed. Siddik. Department of EEE, Raghu Institute of Technology, Visakhapatnam, India,

G. JogaRao. Department of EEE, Raghu Institute of Technology, Visakhapatnam, India,

D.V.N. Ananth. Department of EEE, Raghu Institute of Technology, Visakhapatnam, India,

This paper describes the modeling and control approach of a permanent magnet brushless dc motor. The bridgeless BLDC motor control and operation is discussed in the section 2. The section 3 describes the operation of zeta converter and its state-space representation. The section 4 discusses the PFC of CUK converter and its operation. The results are discussed in section 5 followed by conclusions and references.

II. THE SPEED AND TORQUE CONTROL SCHEME OF BRIDGELESS-ZETA BLDC DRIVE

The configuration of ZETA chopper based bridgeless drive for the brushless dc motor scheme is shown in Fig.1(i). The input ac supply is passed initially though a resonant inductor-capacitor combination circuit and anti-parallel diodes in the phase and neutral as shown. These diodes help to conduct only in one direction at a time and also for ac supply to dc supply conversion without the use of bridge application during each half cycle. During one half cycle, one IGBT will be on and the other off. The switching operation during the positive half cycle is shown in Fig. 1(ii) (a) and in the negative half cycle is shown in the negative half cycle is shown in Fig. 1(ii) (b) [19].

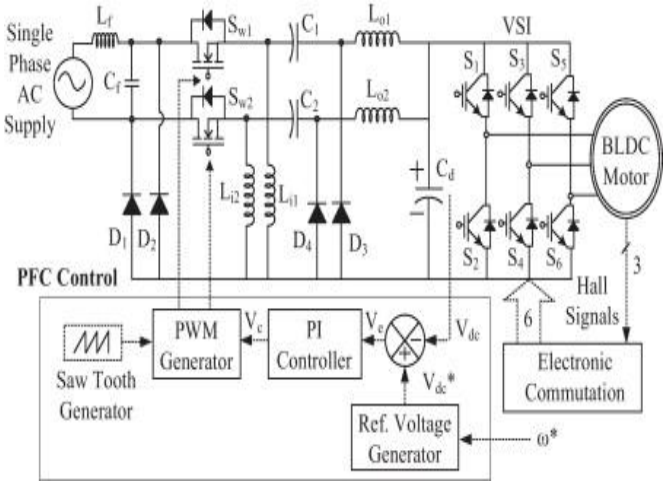

Fig.1(i). ZETA based bridgeless BLDC drive system block diagram

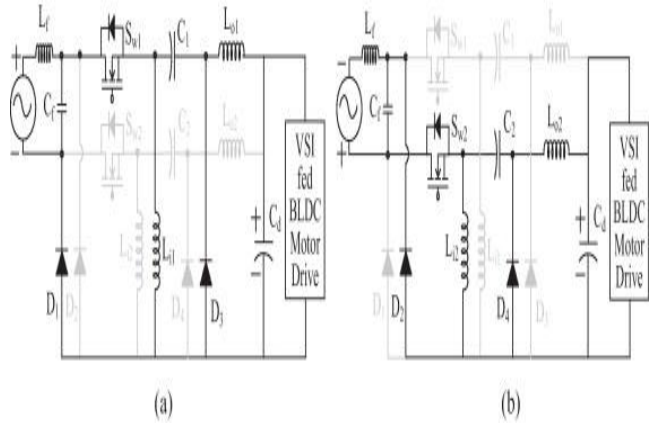

Fig. 1(ii) (a) positive half cycle operation and Fig. 1(ii) (b) negative half cycle operation [19]

In the Fig. 1(ii) (a) during the positive half cycle, the switch Sw1, Li1 and D1 will form a closed path and will complete one half cycle continuous current flow based on the switching duty cycle. The capacitance C1, Lo1 and D3 will help in maintaining constant dc link voltage across the capacitor as per the required or specified dc link voltage (V_{dc}^{*}) and also behave as boost converter drive operation. The same negative cycle operation can be assumed to operate symmetrically like in the positive cycle. The Hall Effect sensor voltage and BLDC motor winding emf voltage in each phase is shown in the Fig.2a. Here each sector operates for 60° for 5 operating sector from zero to five with different switching combination is also shown in the figure. In the sector zero, the switches Q1 and Q5 operate and hall state is 4, A-phase winding is positive high, B phase is negative high and the C phase emf is changing from positive high to negative high in a ramp shape. The same analysis holds good for the other hall states and sectors. The typical BLDC motor winding impedance and emf equivalent circuit is shown in Fig.2(b).

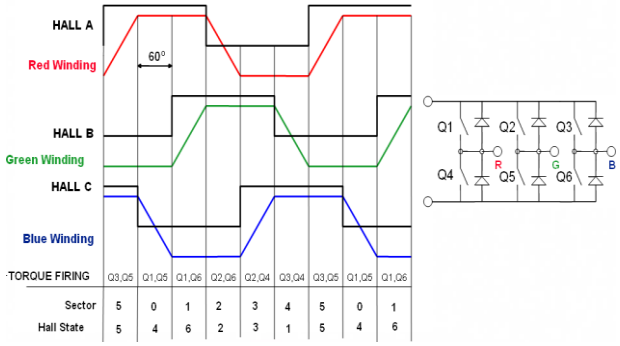

Fig.2a. BLDC three phase voltages, sector selection and Hall states

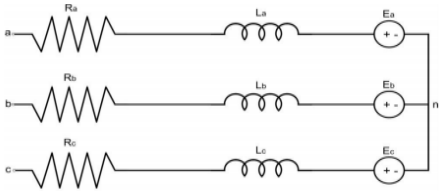

Fig.2b Typical BLDC motor equivalent circuit [21]

Here, among the three phases of the BLDC, only two phases will be switched on at a time and the other is considered to be in the off state. However, desired higher starting and operating torques will be achieved by energizing two rotor position phases. In this, each switch operates for 60° electrical based on the position sensor signal generation based on rotor position. The ideal three phase trapezoidal waveform so produced is shown in Fig.2(a), based on these, the back emf line voltages V_{ab}, V_{bc} and V_{ca} represented as eq. (1a) to (1c).

$$v_{ab} = R(i_a - i_b) + L\frac{d(i_a - i_b)}{dt} + e_a - e_b \quad \text{..... (1a)}$$

$$v_{bc} = R(i_b - i_c) + L\frac{d(i_b - i_c)}{dt} + e_b - e_c \quad \text{..... (1b)}$$

$$v_{ca} = R(i_c - i_a) + L\frac{d(i_c - i_a)}{dt} + e_c - e_a \quad \text{..... (1c)}$$

The electromagnetic torque equation is depicted in equation (2). Here, the three phase currents are represented as i_a, i_b and i_c. The three phases are assumed to have equal resistance and inductance represented with R and L. The three phases back emf is represented as e_a, e_b and e_c.

$$T_e = k_f w_m + J\frac{dw_m}{dt} + T_L \text{..... (2)}$$

The rotor Inertia (J) in gcm^2 and the load Torque is T_L in mNm with friction Constant (K_f), torque constant (Kt) and back-emf constant is (Kb) in Nms.

The back emf of phases a, b and c are shown in equations (3a) to (3c) ad a function of back emf constant and trapezoidal waveform angle factor represented by an angle Electrical Angle (θ_e) and the rotor angle is represented as (θ_m).

$e_a = \frac{k_e}{2} w_m F(\theta_e)$ ..... (3a)

$e_b = \frac{k_e}{2} w_m F(\theta_e - \frac{2\pi}{3})$ ..... (3b)

$e_c = \frac{k_e}{2} w_m F(\theta_e - \frac{4\pi}{3})$ ..... (3c)

The electromagnetic torque (EMT) is represented as torque constant and trapezoidal waveform angle factor represented by an angle θ_e is shown in equation (4).

$T_e = \frac{k_t}{2}[F(\theta_e) i_a + F\left(\theta_e - \frac{2\pi}{3}\right) i_b + + F\left(\theta_e - \frac{4\pi}{3}\right) i_c$ ..... (4)

$\theta_e = \frac{p}{2}\theta_m$ ..... (6)

$F(\cdot)$ gives the Trapezoidal waveform of the BACK EMF.

The trapezoidal waveform angle factor represented during one cycle of operation is shown in Eq (6),

$$F(\theta_e) = \begin{cases} 1, \dots\dots\dots\dots\dots\dots\dots\dots\dots\dots\dots\dots\dots\dots\dots\dots 0 \le \theta_e < \frac{2\pi}{3} \\ 1 - \frac{6}{\pi}\left(\theta_e - \frac{2\pi}{3}\right) \dots\dots\dots\dots\dots\dots\dots\dots\dots\dots\dots\dots \frac{2\pi}{3} \le \theta_e < \pi \\ -1 \dots\dots\dots\dots\dots\dots\dots\dots\dots\dots\dots\dots\dots\dots\dots\dots \pi \le \theta_e < \frac{5\pi}{3} \\ -1 + \frac{6}{\pi}\left(\theta_e - \frac{5\pi}{3}\right) \dots\dots\dots\dots\dots\dots\dots\dots\dots\dots\dots\dots \frac{5\pi}{3} \le \theta_e < 2\pi \end{cases}$$

..... (6)

Under steady state, based on the KCL, the three currents entering into the BLDC motor must be equal to zero as

$i_a + i_b + i_c = 0$ ..... (7)

Using the equation (7), the equations (1) and (2) can be simplified and rewritten as in equations (8a) and (8b) as,

$v_{ab} = R(i_a - i_b) + L\frac{d(i_a - i_b)}{dt} + e_a - e_b$ ..... (8a)

$v_{bc} = R(i_a + 2i_b) + L\frac{d(i_a + 2i_b)}{dt} + e_b - e_c$ ..... (8b)

In the equations (8a) and (8b), the c-phase current is eliminated to minimise the number of variables. Now for simple analysis, state space representation is batter analytical analysis. So, the dynamic state space representation of the two phase currents (a and b), rotor speed and rotor mechanical angles from the equations (8a), (8b), and (6) are shown in the equation (9).

$$\begin{bmatrix} i_a' \\ i_b' \\ w_m' \\ \theta_m' \end{bmatrix} = \begin{bmatrix} -\frac{R}{L} & 0 & 0 & 0 \\ 0 & -\frac{R}{L} & 0 & 0 \\ 0 & 0 & -\frac{k_f}{J} & 0 \\ 0 & 0 & 1 & 0 \end{bmatrix} \begin{bmatrix} i_a \\ i_b \\ w_m \\ \theta_e \end{bmatrix} + \begin{bmatrix} \frac{2}{3L} & \frac{1}{3L} & 0 \\ -\frac{1}{3L} & \frac{1}{3L} & 0 \\ 0 & 0 & \frac{1}{J} \\ 0 & 0 & 0 \end{bmatrix} \begin{bmatrix} v_{ab} - e_{ab} \\ v_{bc} - e_{bc} \\ T_e - T_L \end{bmatrix}$$

…….. (9)

The simplified equation under no input supply voltage and output load torque can be as in equation (10).

$$\begin{bmatrix} i_a' \\ i_b' \\ w_m' \\ \theta_m' \end{bmatrix} = \begin{bmatrix} 1 & 0 & 0 & 0 \\ 0 & 1 & 0 & 0 \\ -1 & -1 & 0 & 0 \\ 0 & 0 & 1 & 0 \end{bmatrix} \begin{bmatrix} i_a \\ i_b \\ w_m \\ \theta_m \end{bmatrix}$$ ..... (10)

Power Losses Calculations:

Any motor power losses are broadly classified as core (Pcore) and copper (PCU) losses. The copper power losses are variable losses and these losses increases with the increase in the winding current produced BLDC motor. It is a function of summation of all phases and fundamental to all phases RMS current represented as in Eq (11). here Ia_i is the ith harmonic current component of a-phase called Ia. The core losses in the BLDC motor is a function of hysteresis (Ph) and eddy current losses (Pe) which are functions of eddy current constant (Ke), hysteresis current constant (Kh), frequency (f), maximum flux density (Bmax) and its weight as depicted by equation (12).

$P_{Cu} = 3R\sqrt{\sum_{i=1}^{\infty} I_{a\_i}^2}$ ..... (11)

$P_{core} = P_e + P_h \cong (k_e f^2 B^2_{max} + k_h f B^2_{max}) * Weight$ ..... (12)

The total eddy current losses to the fundamental eddy current losses is represented by equation (13) and similarly for hysteresis losses is shown in equation (14). These losses are dependent on the RMS of all the voltages from the fundamental to the infinite harmonics existing in the network to the fundamental harmonic voltage. Hence, the parameter is always greater than equal to one.

$\frac{P_e}{P_{e1}} = \sum_{i=1}^{\infty}\left(\frac{V_i}{V_1}\right)^2$ ..... (13)

$\frac{P_h}{P_{h1}} \approx \sum_{i=1}^{\infty}\left(\frac{V_i}{V_1}\right)^2 \frac{1}{i}$ ..... (14)

The resistance and inductance and all the constants and coefficient values are taken at room temperature and pressure. These two equations helps us to evaluate the losses occur in the BLDC motor and the harmonic injection values.

III. PRINCIPLE OF OPERATION OF CONVENTIONAL BRIDGED ZETA CONVERTER

The bridged isolated- ZETA converter is used for step up or down the dc output voltage and also for continuous or discontinuous current mode of operation [22] and [23]. In bridged converter, diode H-bridge converter is used to convert ac power supply to dc supply and the inductors, transformers and capacitor along with the IGBT switch for the operation. The isolated ZETA dc-dc converter is shown in Fig.3(a). There are two modes of operation with switch off as in Fig. 3(b) is first region mode and the other with switch off commonly called as second mode as shown in Fig. 3(b). The disadvantage with the bridged converter is higher losses because of the diode bridge and use of bulky capacitor as described in the Section 1.

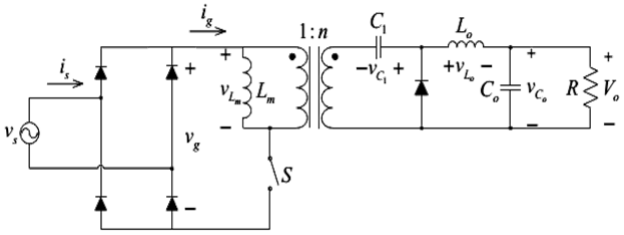

Fig.3(a) Isolated Zeta Converter [23]

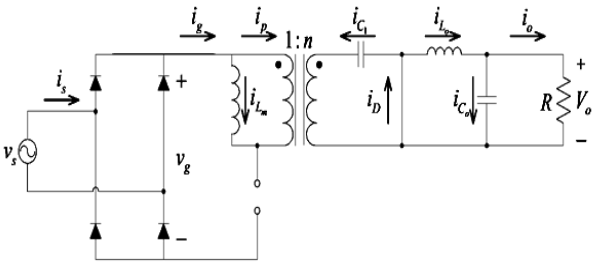

Fig.3(b) Ist Region of operation

In the first mode with IGBT switch is OFF and the diode is ON, the current stored in the input inductor Lin is transformed during positive or negative half cycle using 1:n winding ratio transformer. This current is passed to load circuit using the CLC passive combination as shown. In the other mode, the switch is ON and the second side diode (D) id off, here both source currents along with the inductor current is transformed by the transformer combination action.

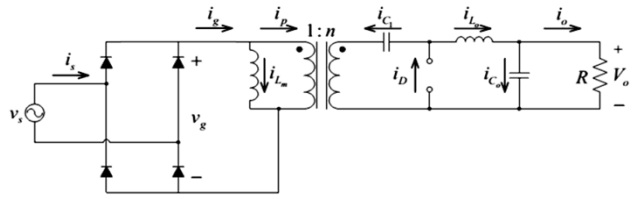

Fig.3(c) 2nd Region of operation

3.1 State Space Averaged Model of Proposed Zeta Converter:

The state-space representation of the switching cycle is shown in equation (15) where the converter conduction or on state is represented as t_{on} and non-conducting or off-time is denoted as (1-d_1) T_s or d_1T_s, and t_{off} respectively.

$$\dot{x} = A_s x + B_s u \text{ and } y = C_s x \quad \text{..... (15)}$$

Where,

$A_s = [A_1d_1 + A_2 (1 – d_1)]$, $B_s = [B_1d_1 + B_2 (1 – d_1)]$ and $C_s = [C_1d_1 + C_2 (1 – d_1)]$ ..... (16)

Using the linearization technique to the equation (16) taking into account small-signal perturbations as $x = X + \tilde{x}$,$y = Y + \tilde{y}$, $d_1 = D + \tilde{x}$, $u = U + \tilde{u}$ be substituted into Eq.(15).

where X >> $\tilde{x}$, Y >> $\tilde{y}$, U >> $\tilde{u}$, D_1 >> $\tilde{D_1}$.

During norming condition, the state equations with the variables are written as in eq (17) to (19) as,

$$X = A_{av}X + B_{av} U = 0; Y = C_{av}X \quad (19)$$

$$A_{av}\tilde{x} + [(A_1+A_2) X + (B_1+B_2) U] \tilde{d} + B_{av} \tilde{u} \quad (20)$$

$$\tilde{y} + C_{av}\tilde{x} + [(C_1-C_2) X] \tilde{d} \quad (21)$$

Where,

$A_{av} = A_1D_1 + A_2 (1 – D_1)$, $B_{av} = B_1D_1 + B_2 (1 – D_1)$ and $C_{av} = C_1D_1 + C_2 (1 – D_1)$ (22)

From Eq. (19),

$X = -A_{av}^{-1} B_{av}U$; and $\frac{Y}{U} = -C_{av} A_{av}^{-1}B_{av}$ (23)

Applying Laplace transform to Eq.(23), we get the equation (24a) and (24b) as

$\dot{x} = [sI - A_{av}]^{-1}[B_{av} \tilde{V_g}(s) + [(A_1 - A_2) X + (B_1 - B_2) V_g] \tilde{d_1}(s)]$ (24a)

$\tilde{y}(s) = C_{av} \tilde{x}(s) + [(C_1 - C_2)X] \tilde{d}(s)$ (24b)

Dividing the equation (24b) with (24a) to get output to input which is the transfer function model of the equations for $n \tilde{V_g}$ = zero or (0). It is the overall system transfer function as shown in (25) describes the property under normal steady-state value.

$$\frac{\tilde{y}(s)}{\tilde{d_1}(s)} = C_{av} [sI - A_{av}]^{-1} [(A_1 - A_2) X + (B_1 - B_2) V_g + (C_1 - C_2)X] \quad (25)$$

Now considering any disturbance or noise input to the circuit is zero as denoted by $\tilde{d_1}$ = 0, we get Eq (26)

$$\frac{\tilde{y}(s)}{\tilde{V_g}(s)} = C_{av} [sI - A_{av}]^{-1} C_{av} \quad (26)$$

IV. DESIGN OF A PFC CUK CONVERTER

A dc link based voltage control with discontinuous modes of operation for a PFC based CUK converter for a BLDC motor drive is shown in Fig. 4 and Fig.5 [14]. The discontinuous current conduction mode three switching operating intervals are shown in Fig. 4(a), 4(b) and 4(c) and the operating circuit waveform is shown in the Fig.4(d). In the first interval as in Fig.4(a), the IGBT switch is ON, diode (D) is off and the charging inductor (Lo) is path for the current to pass through it to the load. In this mode as the current is reaching the load capacitor and resistor, the capacitor is charged. In the second mode, the IGBt is OFF, the reverse diode (D) is conducting and the inductor (Lo) is discharging and supplying current to the load as in Fig.4(b) and in this mode also, load capacitor is charging. In the third operating mode, the IGBT is OFF and also the inductor Lo is open as the total current is passed through the low resistance path via diode as in Fig.4(c). As the inductor is fully discharged, this Lo inductor cannot supply current to the load. So, in this interval, the capacitor is discharged and will supply current to the load and this value is decaying component. The CUK converter operation is for boosting voltage and for discontinuous mode of operation. If the circuit is to be used for the conduction mode, the passive elements like input and output inductors (Li and LO) and the intermediate capacitor C1 all must be conducting. The dc link voltage (Vdc) equation in terms of duty cycle (D) and input voltage (Vin) derivation and the duty cycle value in terms of input and output voltage parameters are now explained. The supply voltage (Vs) applied to the diode bridge rectifier is shown in equation (27) as function of maximum voltage (Vm) and fundamental frequency of the line (fL) at the time (t).

Here 220 volts and 50 Hz system is considered for analysis, and the final value is

$$v_s(t) = V_m \text{Sin}(2\pi f_L t) = 220\sqrt{2}\,\text{Sin}(314t)\text{V} \quad (27)$$

The equation (27) can also be rewritten as in equation (28) with instantaneous input voltage (Vin(t)) given to the diode bridge in terms of magnitude value is denoted in equation (28) with modulus function as represented by | |

$$V_{in}(t) = |V_m \text{Sin}(\omega t)| = |220\sqrt{2}\,\text{Sin}(314t)|\text{V} \quad (28)$$

The output dc voltage of the Cuk converter (V_{dc}) in terms of duty cycle (D) and input voltage (Vin) is given in equation (29)

$$V_{dc} = \frac{D}{(1-D)} V_{in}(t) \quad (29)$$

The instantaneous of duty cycle D(t) is a function of the ratio of output dc link voltage across the resistor (Vdc) and sum of instantaneous input voltage Vin (t) and output dc voltage as denoted by equation (30) as and rearranging it will be,

$$D(t) = \frac{V_{dc}}{V_{in}(t) + V_{dc}} = \frac{V_{dc}}{|V_m Sin(\omega t)| + V_{dc}} \quad (30)$$

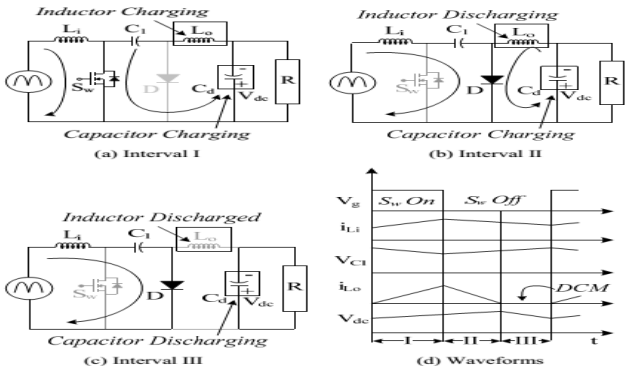

Fig. 4(a) to 4(c) CUK converter in discontinuous current mode operation during different switching modes of the IGBT switch, diode, and the inductor (Lo) and Fig.4(d) its associated waveforms [14]

The minimum (Vdcmin) and maximum (Vdcmax) operating voltages are assumed to be 40V and 220V for the CUK dc-dc chopper with PFC objective with maximum power rating of 350W (P max) and the switching frequency (fS) is 20KHz and the analysis is done for an operating wattage of 250W is considered for the analysis. The continuous or discontinuous current mode of operation, the passive parameters is designed as follows. The input inductance during the continuous conduction mode (Lic) as a function of Vin(t), D(t), Iin(t) and fs or in terms of power or resistance or in terms of input and output voltages is denoted in (31)

$$L_{ic} = \frac{V_{in}(t)D(t)}{2I_{in}(t)f_S} = \frac{R_{in}D(t)}{2f_S} = \left(\frac{V_s^2}{P_i}\right)\frac{D(t)}{2f_S}$$
$$= \frac{1}{2f_S}\left(\frac{V_s^2}{P_i}\right)\left(\frac{V_{dc}}{V_{in}(t)+V_{dc}}\right) \quad (31)$$

It can be observed from the equation (31), the inductance value depends on the square of the supply voltage or its rms value. In the design, under worst case, with the minimum or lower supply voltage (i.e. Vs or Vs min equal to 40V) and for the peak value of supply voltage (200V) to get the maximum DC link voltages, the continuous current conducting mode input inductor value is found by using formula in the equation as in (32a) for 200 volts input supply and for 40 volts input supply as given in equation (32b),

$$L_{ic200} = \frac{1}{2f_S}\left(\frac{V_{smin}^2}{P_{max}}\right)\left(\frac{V_{dcmax}}{\sqrt{2}V_{smin} + V_{dcmax}}\right) \quad (32a)$$

$$L_{ic40} = \frac{1}{2f_S}\left(\frac{V_{smin}^2}{P_{min}}\right)\left(\frac{V_{dcmin}}{\sqrt{2}V_{smin} + V_{dcmin}}\right) \quad (32b)$$

Hence from the equations (32a) and (32b), the input inductor values with lower and higher input voltage values changes with the minimum (Pmin) and maximum power (Pmax) rating values for that voltage values. Now the same circuit with discontinuous conduction mode and with voltage control mode of operation, the three interval modes are represented as in Fig.5(a) to Fig.5(c) and the associated waveforms is shown in Fig.5(d). The analysis of the circuit with this voltage mode is similar to current mode explained for Fig.4.

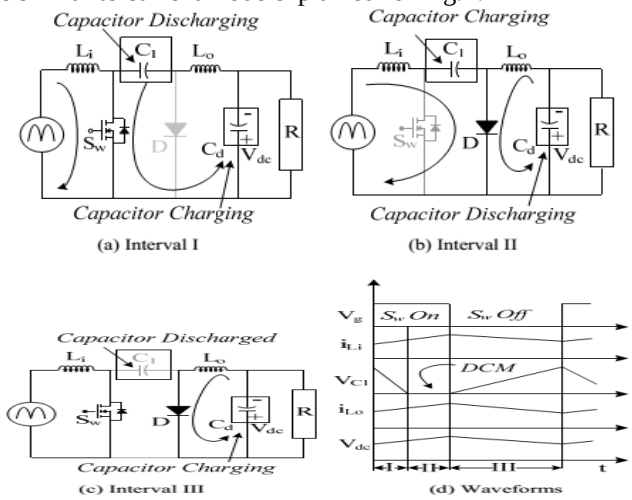

Fig. 5(a) to 5(c) CUK converter in discontinuous voltage control mode operation during different switching modes of the IGBT switch, diode, and the intermediate capacitor (C1) and Fig.5(d) shows its associated waveforms [14]

V. SIMULATION RESULTS & DISCUSSION OF A PROPOSED ZETA CONVERTER

A 7.5N-m, 300 rad/min, 220V rating BLDC motor is considered for analysis. Both the ZETA and the CUK converters can stepup voltage to 500V dc. The PI controller values for dc voltage are taken after tuning is 0.013 and 16.61 and for the speed controller, the PI controller values are 139.720 and 54.6363. The source voltage and current waveforms with zeta and cuk converter are shown in Fig. 6(a). In this the both zeta and cuk converter voltages are sinusoidal, voltage and currents are in phase to each other. However, with zeta, the current is more sinusoidal than with CUK due to dominating inductor and with more advanced control action.

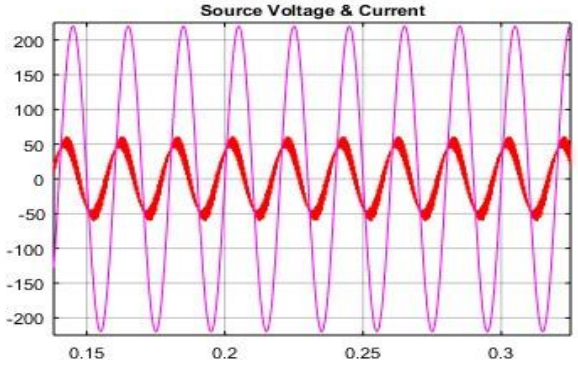

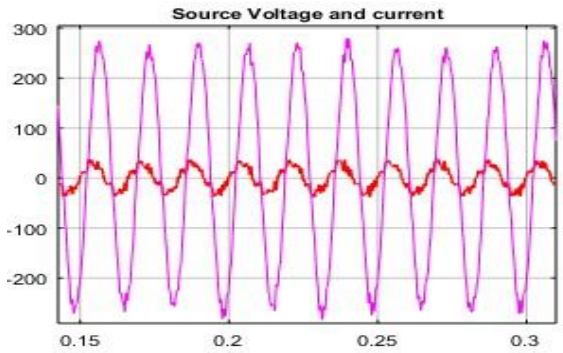

Fig.6(a) Source voltage and current waveforms with (i) ZETA and (ii) CUK

The dc link capacitor voltage before the inverter terminal with zeta and cuk converter is shown in Fig 6(b). The boost characteristics and ripples characteristics are found more satisfactory with zeta than with cuk converter even though almost same control strategy and motor loads are adopted. The IGBT based inverter voltage and current waveforms are shown in Fig. 6(c). It can be observed that the voltage and current are almost alike with both the choppers, but there is small drop in voltage when load torque on the BLDC increased at 0.4s with cuk converter, where is constant with zeta converter. The BLDC motor parameters like stator-A-phase current, rotor speed and torque are shown with zeta and cuk converter as in Fig. 6(d). Here the parameters and outputs are same with both the choppers and the only difference is at the source power factor and voltage and current waveforms.

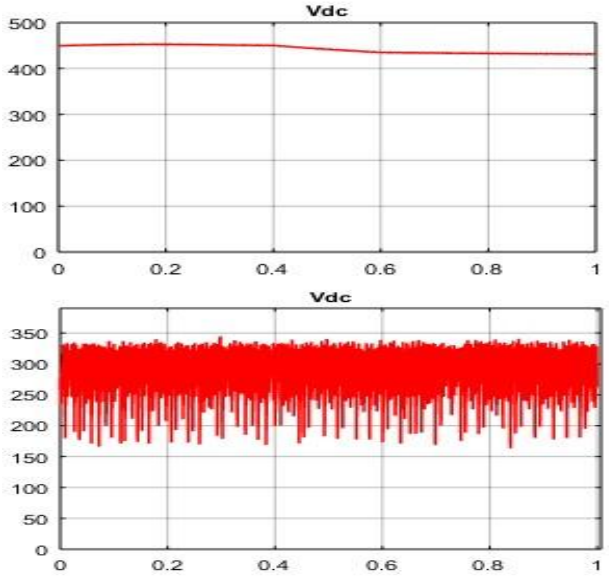

Fig.6(b) DC link capacitor voltage waveform with (i) ZETA and (ii) CUK

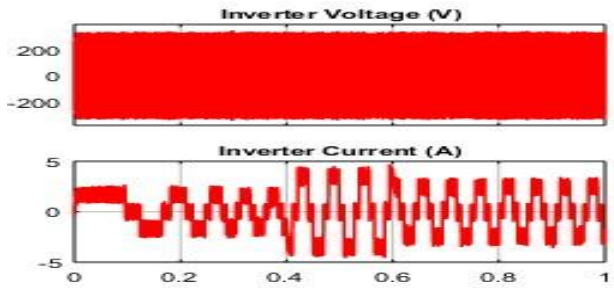

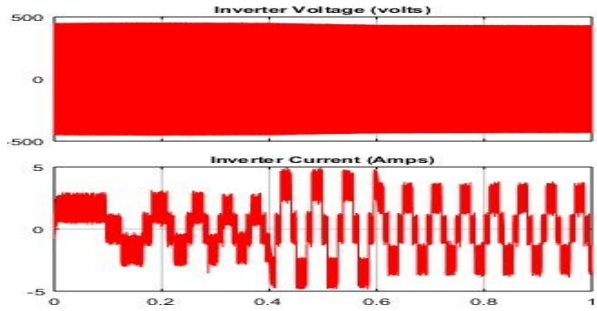

Fig.6(c) Inverter voltage and current waveforms with (i) ZETA and (ii) CUK

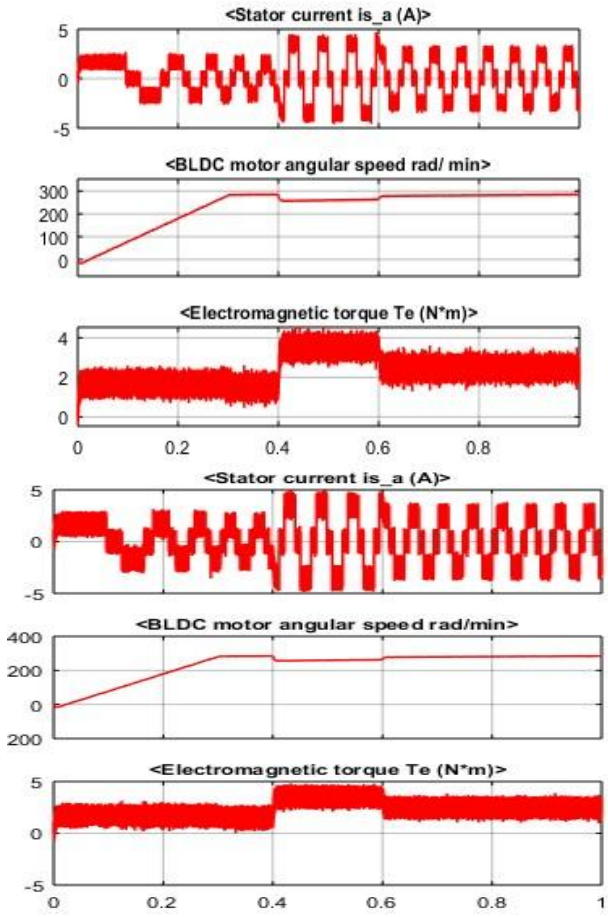

Fig.6(d) BLDC motor current, rotor speed and torque waveforms with (i) ZETA and (ii) CUK

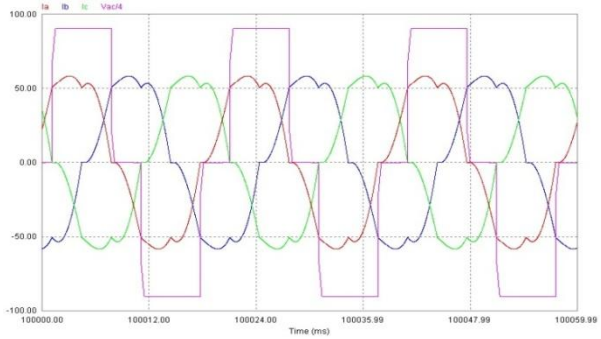

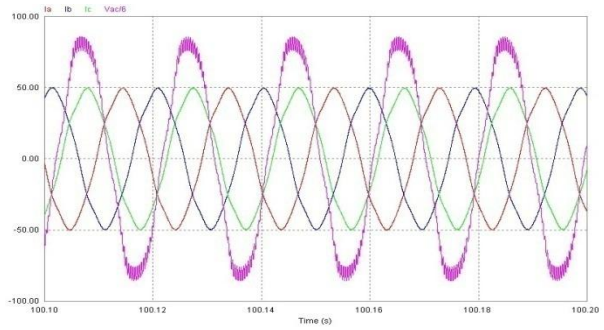

Fig. 7a BLDC voltage and current waveforms with (i) CUK and (ii) ZETA chopper circuit

The BLDC inverter voltage and current after the filter with cuk chopper is shown in Fig.7a(i) and using zeta converter as shown in Fig.7a(ii). Here A-phase voltage and three phase currents are compared for the analysis. In this, the voltage is square wave for cuk converter and sinusoidal with zeta. The current is having some harmonic components, but the current is in-phase with the same phase voltage. The THD values of current and voltage are shown in Fig.8(a) and 8(b) using cuk converter. The current THD is 10.68% and voltage is 29.15% with harmonic order of 5, 7, 11, 13, 17 and 19 significant.

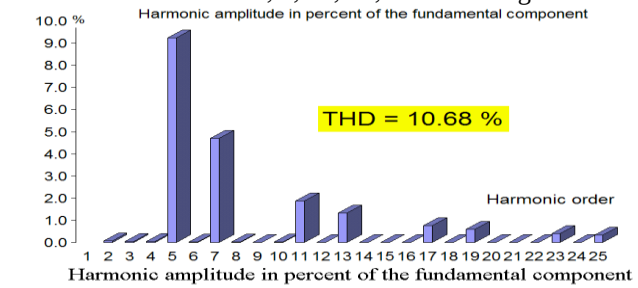

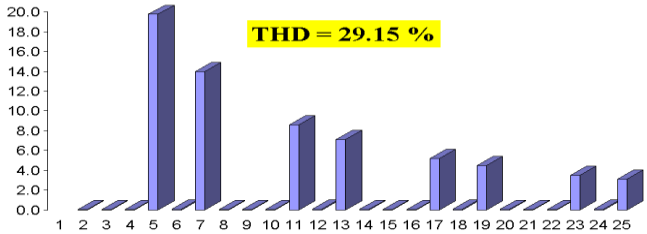

Fig. 8(a). BLDC output currents and Fig.8(b). Harmonic content of the BLDC output voltage with CUK

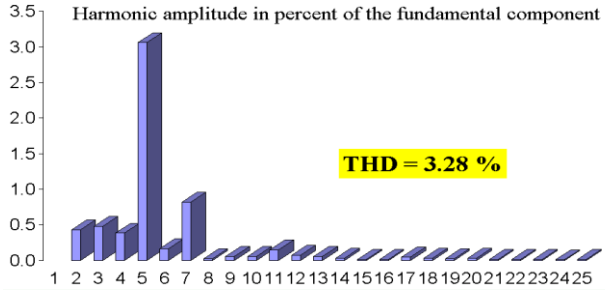

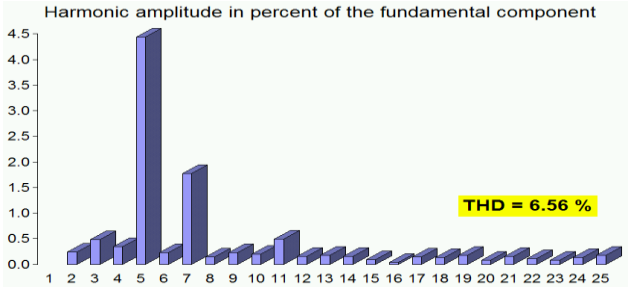

Fig. 9(a). BLDC output currents and Fig.9(b). Harmonic content of the BLDC output voltage with ZETA.

A comparison of the conventional ZETA as in Fig.3, cuk converter as in Fig.4 and zeta converter in Fig.1 showing different losses and efficiency is denoted in Table 1. Comapred to the combination, the proposed ZETA converter is better in terms of THD, PFC, and also in terms of efficiency.

Table- I: . BLDC core, copper, friction and windage losses in (W) and efficiency in (%)

Topology	Copper Losses	Core Losses	Friction & Windage losses	Cumulative losses	Overall efficiency of the drive
Rated	1701.15	219.40	120	2040.55	90.74
Conventional ZETA in Fig.3	2318.93	180.82	120	2619.75	88.42
CUK Converter in Fig.4	1724.73	251.32	120	2096.05	90.51
ZETA Converter in Fig.1	1486.33	269.96	120	1876.29	91.42

VI. CONCLUSION

The work describes the power factor correction in case of a BLDC drive load application and also to reduce the power losses occur in the motor. For this, bridged ZETA converter and a bridgeless CUK and ZETA converters are compared for the analysis. For the same input source voltage and same load on the BLDC motor, the input voltage and current are almost in phase with both bridgeless ZETA and CUK, while the later current waveform is little distorted.

Also, the dc link capacitor voltage with ZETA is having lower ripples and also constant even with large change in the load torque. The CUK converter dc link voltage is having considerable ripples. The current THD as well as the voltage THD are better with bridgeless ZETA than with the CUK. The overall losses is lesser and higher efficiency is observed with bridgeless ZETA than with the bridgeless CUK and bridged (H-bridge based two stage) ZETA is having more losses. Hence in all ways the bridgeless ZETA is found better and efficient for the BLDC motor drive application.

REFERENCES

1. Du, Yi, Liang Du, Bin Lu, Ronald Harley, and Thomas Habetler. "A review of identification and monitoring methods for electric loads in commercial and residential buildings." In 2010 IEEE Energy Conversion Congress and Exposition, pp. 4527-4533. IEEE, 2010.
2. Fu, Dianbo, Fred C. Lee, Yang Qiu, and Fred Wang. "A novel high-power-density three-level LCC resonant converter with constant-power-factor-control for charging applications." IEEE Transactions on Power Electronics 23, no. 5 (2008): 2411-2420.
3. Zeng, Zheng, Huan Yang, Shengqing Tang, and Rongxiang Zhao. "Objective-oriented power quality compensation of multifunctional grid-tied inverters and its application in microgrids." IEEE transactions on power electronics 30, no. 3 (2014): 1255-1265.
4. Garland, David. "Penal power in America: Forms, functions and foundations." Journal of the British Academy 5 (2017): 1-35.
5. Bist, Vashist, and Bhim Singh. "An adjustable-speed PFC bridgeless buck–boost converter-fed BLDC motor drive." IEEE Transactions on Industrial Electronics 61, no. 6 (2013): 2665-2677.
6. Gopinath, M., and D. Yogeetha. "Efficiency analysis of bridgeless PFC boost converter with the conventional method." International Journal of Electronic Engineering Research 1, no. 3 (2009): 213_221.
7. Yadav, Apoorva, and Arunima Verma. "Sepic DC–DC Converter: Review of Different Voltage Boosting Techniques and Applications." In 2020 2nd International Conference on Innovative Mechanisms for Industry Applications (ICIMIA), pp. 733-739. IEEE, 2020.
8. Musavi, Fariborz, Wilson Eberle, and William G. Dunford. "A phase-shifted gating technique with simplified current sensing for the semi-bridgeless AC–DC converter." IEEE Transactions on Vehicular Technology 62, no. 4 (2012): 1568-1576.
9. Siu, Ken KM, and Carl NM Ho. "A critical review of Bridgeless PFC boost rectifiers with common-mode voltage mitigation." In IECON 2016-42nd Annual Conference of the IEEE Industrial Electronics Society, pp. 3654-3659. IEEE, 2016.
10. Vishvanath, M., and R. Balamurugan. "An Review of Power Factor Correction in SRM Drives Using Bridgeless Converters." Telkomnika Indonesian Journal of Electrical Engineering 14 (2015).
11. Ma, Hongbo, Yuan Li, Jih-Sheng Lai, Cong Zheng, and Jianping Xu. "An improved bridgeless SEPIC converter without circulating losses and input-voltage sensing." IEEE Journal of Emerging and Selected Topics in Power Electronics 6, no. 3 (2017): 1447-1455.
12. Mahdavi, Mohammad, and Hosein Farzanehfard. "Bridgeless SEPIC PFC rectifier with reduced components and conduction losses." IEEE Transactions on Industrial Electronics 58, no. 9 (2010): 4153-4160.
13. Singh, Bhim, and Vashist Bist. "Power-quality improvement in PFC bridgeless SEPIC-fed BLDC motor drive." International Journal of Emerging Electric Power Systems 14, no. 3 (2013): 285-296.
14. Singh, Bhim, and Vashist Bist. "Improved power quality bridgeless Cuk converter fed brushless DC motor drive for air conditioning system." IET Power Electronics 6, no. 5 (2013): 902-913.
15. Yang, Hong-Tzer, Hsin-Wei Chiang, and Chung-Yu Chen. "Implementation of bridgeless Cuk power factor corrector with positive output voltage." IEEE Transactions on Industry Applications 51, no. 4 (2015): 3325-3333.
16. Singh, Bhim, Vashist Bist, Ambrish Chandra, and Kamal Al-Haddad. "Power factor correction in bridgeless-Luo converter-fed BLDC motor drive." IEEE Transactions on Industry Applications 51, no. 2 (2014): 1179-1188.
17. Singh, Bhim, and Radha Kushwaha. "An EV battery charger with power factor corrected bridgeless zeta converter topology." In 2016 7th India International Conference on Power Electronics (IICPE), pp. 1-6. IEEE, 2016.
18. Khan, Shakil Ahamed, Nasrudin Abd Rahim, Ab Halim Abu Bakar, and C. K. Tan. "Single-phase bridgeless Zeta PFC converter with reduced conduction losses." Journal of Power Electronics 15, no. 2 (2015): 356-365.
19. Singh, Bhim, and Vashist Bist. "Power quality improvements in a zeta converter for brushless DC motor drives." IET Science, Measurement & Technology 9, no. 3 (2014): 351-361.
20. Salehifar, Mehdi, Ghanim Putrus, and Peter Barras. "Analysis and comparison of conventional two-stage converter and single stage bridgeless ac-dc converter for off-road battery charger application." (2016): 7-7.
21. G. Joga Rao, D.V.N. Ananth, P.Kiran Kumar, P.RamReddy, "Performance Enhancement of PMBLDC Motor Drive by Multi-Carrier Modulation Technique", International Journal of Innovative Technology and Exploring Engineering (IJITEE), 8 (7), May, 2019.
22. Bist, Vashist, and Bhim Singh. "A brushless DC motor drive with power factor correction using isolated zeta converter." IEEE Transactions on Industrial Informatics 10, no. 4 (2014): 2064-2072.
23. Kushwaha, Radha, and Bhim Singh. "UPF-isolated zeta converter-based battery charger for electric vehicle." IET Electrical Systems in Transportation 9, no. 3 (2019): 103-112.

AUTHORS PROFILE

Syed. Siddik is doing his MTECH in power electronics from Raghu institute of technology (Autonomous) Visakhapatnam. He received B.Tech Electrical and electronics Engineering from Chirala Engineering College, Chirala. His favorite topics include Power electronics, IOT and Renewable electrical systems.

Dr. G Joga Rao is working as an associate professor in the department of EEE, Raghu Institute of Technology (Autonomous) Visakhapatnam. He obtained B.Tech (Electrical Engineering) and M.Tech (Electrical Power Engineering) degree from J.N.T University, Hyderabad, in 2004 and 2007 respectively. He completed his doctoral program from S.R University, India in 2017. He has more than 15 years of teaching experience in various colleges and published more than 50 publications in various reputed international journals. His area of interest includes Energy Systems, Power Electronics and Renewable Energy Technologies. He is a life member of the Indian Society for Technical Education and Institute of Engineers IE(I)

D.V.N. Ananth was born in Visakhapatnam, India on 20th August 1984. He received B.Tech Electrical Engineering from Raghu Engineering College, Visakhapatnam and M.Tech from Sreenidhi Institute of Science & Technology, Hyderabad, India. He is working as an Assistant Professor in Electrical Department, Raghu institute of technology (Autonomous) Visakhapatnam. His favorite topics include Renewable electrical systems, industrial drives, power systems, power electronics, control systems, HVDC systems and Reactive power compensation techniques.